ACS Catalysis

RESEARCH ARTICLE

pubs.acs.org/acscatalysis

Aerobic Oxidation of Hydrocarbons Catalyzed by Mn-Doped Nanoporous Aluminophosphates (II): Hydroperoxide *Decomposition*

Luis Gómez-Hortigüela,* Furio Corà,* and C. Richard A. Catlow

Department of Chemistry, University College London, 20 Gordon Street, WC1H 0AJ London, United Kingdom

ABSTRACT: Electronic structure methods based on hybrid-exchange functionals in Density Functional Theory (DFT) and periodic boundary conditions have been applied to study the reaction mechanism of the aerobic oxidation of hydrocarbons catalyzed by Mn-doped nanoporous aluminophosphates. In this paper we examine the decomposition of hydroperoxide intermediates (ROOH). The reaction takes place on Mn^{II} acid sites, charge-balanced by a proton on a nearest neighbor framework oxygen, resulting from the *preactivation* step. In this stage, the Mn^{II} sites catalyze the homolytic *decomposition* of the hydroperoxide molecules to produce Mn^{III} and oxo-containing radical species, stabilized by complexation to Mn^{III}, yielding in addition alcohol and water molecules. Two parallel reaction pathways have been identified for this process, through alkoxy (RO·) or hydroxy (HO·) radical-like intermediates. The occurrence of the two mechanisms depends on the stereochemistry of the initial adsorption of ROOH onto the active site, which takes place through H-bonding with the framework acid proton: adsorption via the hydroxylic O atom of ROOH leads to RO· intermediates, while adsorption via the nonterminal O atom in ROOH, which is less energetically stable, drives the decomposition toward HO· intermediates. In both cases, the hydroperoxide decomposition is assisted by the Mn^{II} sites, in a concerted mechanism that consists of a H-transfer from the framework to the O atom of the adsorbed ROOH involved in the H-bond, prompting the oxidation of Mn^{II}, and the O−O homolytic cleavage in ROOH, leading to the formation of RO· or HO· radicals that are stabilized by binding the oxidized Mn^{III} site. The relative energetics of the two reaction pathways is explained in terms of the relative stability of the oxo-radicals produced: the higher stability of RO· radicals causes a more favorable *decomposition* of the hydroperoxide intermediate through this pathway. Our results demonstrate the crucial role of Mn in this stage of the aerobic oxidation of hydrocarbons, due not only to its redox activity but also, and fundamentally, to its coordinative unsaturation, that allows for the stabilization of the radicals produced by complexation.

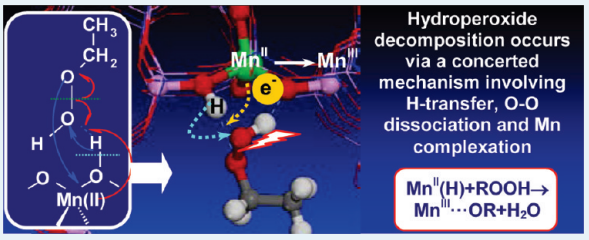

KEYWORDS: oxidation, heterogeneous catalysis, nanoporous aluminophosphates, zeolites, molecular modeling, hydroperoxide, reaction mechanism

INTRODUCTION

The selective oxyfunctionalization of saturated hydrocarbons, especially using O_2 as the oxidant, represents a major challenge in contemporary catalytic chemistry, and has spurred an intensive search in particular for efficient heterogeneous selective oxidation catalysts able to sustain the process on an industrial scale. Crystalline nanoporous aluminophosphates (AlPOs), analogous to zeolites but where Si ions are replaced by Al and P,[1] were found to be active when doped with transition metals such as Co, Mn, and Fe.[2−4] These materials combine the redox activity of the transition metal cations—able to adopt II and III oxidation states—with the unique spatial environment imposed by the molecular dimensions of their crystalline porous network,[5−8] making them very efficient and selective catalysts for a wide range of oxidation reactions, including the industrially fundamental selective oxidations of *n*-hexane[7−10] and cyclohexane,[11−17] the epoxidation of alkenes,[18] and the Baeyer−Villiger oxidation of ketones to lactones,[19] all using O_2 as the oxidant.

The aerobic oxidation of cyclohexane catalyzed by MnAPO-5, a Mn-doped aluminophosphate with the AFI framework structure, has been the subject of in-depth mechanistic experimental investigations by Iglesia and co-workers.[14] Although there is evidence for the occurrence of a free-radical mechanism when using Co-, Fe-, and Mn-containing AlPO catalysts,[7,14,20] the exact details of this oxidation reaction remain unknown. Many of the intermediates involved in the oxidation mechanism lack the stability and lifetime required to be detected and analyzed in situ; hence, it is difficult, if not impossible, to characterize them solely using experimental techniques. Besides, energetic information, both reaction enthalpies and activation energies, is difficult to obtain experimentally. This mechanistic and energetic information can instead be gained from contemporary computational electronic-structure methods, as long as reliable models for the catalysts are available, providing an excellent complementary tool for mechanistic experimental studies.

In free-radical autoxidations catalyzed by transition-metal-doped AlPOs, the role of the redox-active sites has generally been proposed to be the homolytic decomposition of alkyl hydroperoxide intermediates (ROOH) via Haber−Weiss mechanisms[21−23] to form chain-initiating alkoxy (RO·) and

Received: February 28, 2011
Revised: May 13, 2011
Published: June 28, 2011

Scheme 1. Decomposition of ROOH by Transition Metal Sites in AlPOs

$$1)\ ROOH + Me^{II}OH \rightarrow RO^{\cdot} + Me^{III}O + H_2O$$

$$2)\ ROOH + Me^{III}O \rightarrow ROO^{\cdot} + Me^{II}OH$$

alkylperoxy (ROO·) radicals that will undergo new *propagation* reactions. Such a decomposition can in principle take place through the reduced (1) or oxidized (2) transition metal cations (Me) (Scheme 1), prompting in each case a redox-process (oxidation or reduction, respectively) of the active site.

Following the reaction scheme proposed in ref 14, we reported an overview of the complete reaction mechanism for the aerobic oxidation of ethane catalyzed by Mn-doped AlPO-5, obtained by Density Functional Theory (DFT) methods.[24] Our computational study allowed us also to examine alternative mechanistic pathways to those proposed in ref 14, whose occurrence is difficult to characterize experimentally. In that paper, we showed that the main catalytic cycle requires the simultaneous presence of Mn^{II} and Mn^{III} sites, each with a particular function along the reaction path. We proposed a *preactivation* step (I), in which the original Mn^{III} sites present in the calcined catalyst are transformed in Mn^{II} and Mn^{III}-peroxo complexes, both of which are required species for the subsequent set of reactions.[25] The Mn^{III}-peroxo complexes are involved in the production of the hydroperoxide intermediate ROOH. *Decomposition* of this hydroperoxide can only take place through reduced Mn^{II} sites (1) (Scheme 1), since reaction 2, namely, decomposition of ROOH through Mn^{III} sites to give peroxo radicals, is a very unfavorable process.[25] Thus, only the reduced Mn^{II} sites, resulting from the *preactivation* step, catalyze the *decomposition* of the hydroperoxide intermediates into alcohol and water molecules, leading to the production of oxo-type radicals. These radicals will then be responsible for the activation of new hydrocarbon molecules in subsequent reaction steps, yielding finally Mn^{III}-peroxo complexes and so providing a link between the two key species produced in the *preactivation* step. In the present paper, which follows our initial report in this series concerning the *preactivation* step (I),[25] we focus on the mechanistic issues of the stage in which the hydroperoxide intermediates enter the reaction cycle by being decomposed through the preactivated Mn^{II} sites into oxidative products and oxo radical-like species. In subsequent papers, we shall report detailed results concerning the activation of hydrocarbon molecules by these oxo-radical species in the *propagation* reactions (III) and, finally, the *regeneration* of the Mn^{II} active sites to close the oxidation cycle (IV). For consistency of notation and ease of reference, here and in future works examining this catalytic reaction, we retain the labeling of intermediates and reaction steps introduced in reference 24.

COMPUTATIONAL METHODOLOGY

The computational methodology is the same as discussed in our previous work in this series.[25] We have selected ethane as the hydrocarbon and the Mn-doped AFI structure (MnAPO-5) as the catalyst to represent the class of aerobic oxidation reactions in Mn-doped AlPOs. The Mn-doped AFI framework is described with periodic boundary conditions, using 1 crystallographic unit cell (72 atoms) in the *P*1 space group with no symmetry and 1 Mn ion (replacing 1 Al) per AFI unit cell (see ref 25). We have performed DFT calculations, as implemented in the CRYSTAL program,[26] using the hybrid-exchange functional B3LYP. A selected number of calculations has been repeated including the empirical dispersion term, following the method proposed by Grimme (B3LYP+D functional).[27,28] Calculations show the high-spin configuration to be the ground electronic state both for Mn^{II} (d^5, with 5 unpaired electrons) and Mn^{III} (d^4, with 4 unpaired electrons). Where Mn^{2+} replaces Al^{3+}, the negative charge is compensated by the presence of a proton attached to one of the four O ions nearest-neighbor to Mn. The most stable location for the proton is when bonded to the O atom shared by the 12- and 4-membered-ring channels; hence, we selected this position as that where the H will be attached in the reduced catalyst.

In the ROOH decomposition step (reaction 1), apart from Mn oxidation, three atomic rearrangements take place: the O−O bond dissociation, the H-transfer reaction, and the approach of the resulting radical to Mn to form a complex. Each of the above rearrangements can in principle be employed to represent the reaction coordinate for the hydroperoxide decomposition; at this stage, however, it is unclear if any of the contributions can be selected as the main driving force for the reaction. To shed light on this issue, we have initially calculated the energy profile along each internal coordinate, by performing constrained geometry optimizations in which the internal coordinate chosen was frozen and modified in discrete steps of 0.1 Å, and all other internal degrees of freedom relaxed. These constrained geometry optimizations, however, did not allow the transformation of the reactants into the products, showing that the decomposition of ROOH takes place via a concerted mechanism, in which the three internal coordinates evolve at the same time. We also noted that on varying only one of the three internal coordinates the electronic structure obtained starting from reagent and product configurations is different, indicating the existence of two distinct and unconnected potential energy surfaces (PESs). Such a simplified procedure is therefore unable to provide even an estimate of the transition state (TS), identified as the point connecting the PES basins of reagents and products.

Accurate transition state (TS) searches require the use of the Hessian (second derivative) matrix of the system, and need to be initiated in a region of the coordinate space in which the PES has the correct curvature. Usually the initial guess of the geometry can be estimated by scanning a reasonably chosen reaction coordinate to locate a local maximum in the PES connecting reagents and products. The presence of two distinct PESs, obtained starting from reagents and products in the present case, makes such a procedure inadequate. We have therefore adopted an iterative sequence of steps, in the following way: first, we performed two sets of constrained geometry optimizations varying only one of the three internal coordinates (and freezing it at intervals of 0.1 Å), but starting from the geometry of the reactants and of the products independently. We then determined the value of this coordinate at which the two energy surfaces (from the reactants and products configurations) intersect, and we identified this as the partial TS for the first internal coordinate chosen. We then repeated a constrained TS search varying a second internal coordinate, but keeping the first frozen at the value determined above, thus identifying the value of the second internal coordinate at the TS. Finally, a similar search has been performed for the third and last internal coordinate, freezing the geometry corresponding to the two other internal coordinates at the values found above, providing in this way a final estimate of the TS structure for the overall process. Since the energy changes

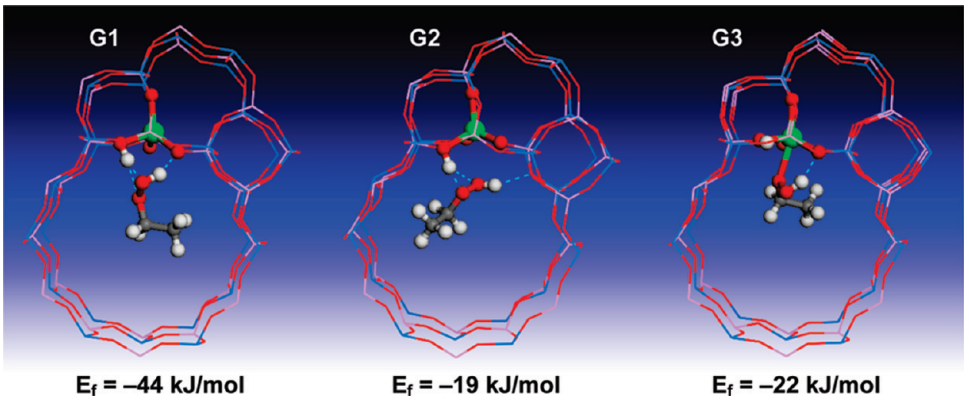

Figure 1. Structure and energy of the three ROOH···Mn^{II} intermediates identified (bottom, formation energies, E_f). **G1** and **G2** involve adsorption through H-bonds between the framework H and either of the two O atoms in ROOH, while **G3** involves complexation of ROOH by Mn^{II}, without direct interaction with the framework H.

associated with modifications of O−O, O···Mn, and O−H bond distances are sufficiently different, this factorization has proven effective in the present case, and has enabled us to locate a region of coordinate space where the Hessian has the correct curvature. Refinement of the final TS structure was performed by eigenvector-following techniques based on a numerical calculation of the Hessian matrix, ensuring the presence of only one negative mode in the final TS. Activation energies and reaction enthalpies for each elementary step are calculated using this TS energy and fully optimized configurations for reactants and products.

The oxidation state of the Mn active site in the different intermediates was identified by comparing the corresponding Mn atomic spin density with those of Mn^{III} (3.79 unpaired electrons, d^4) and Mn^{II} (4.83 unpaired electrons, d^5) in the AFI framework, all obtained with a Mulliken population analysis.

RESULTS

In our earlier overview of the aerobic hydrocarbon oxidation, we identified four subsequent stages in the catalytic reaction mechanism, named as *preactivation*, *hydroperoxide decomposition*, *propagation*, and *regeneration*. As noted, this paper focuses on the *decomposition* step, in which hydroperoxide molecules produced are transformed into oxo-type radicals on preactivated Mn^{II} sites. In the subsequent *propagation* stage, these oxo-radicals will be responsible for the activation of new hydrocarbon molecules through H-transfer, leading to the formation of alkyl radicals that will be stabilized by addition of O_2. A final *regeneration* of the Mn sites by reduction of Mn closes the reaction cycle. In our previous work,[25] we found that decomposition of ROOH on Mn in the oxidized state (III) is unfavorable, and does not provide even a local minimum in the PES. Decomposition must therefore occur on reduced Mn^{II} sites. We have identified two parallel mechanisms whereby hydroperoxide decomposition can take place, via alkoxy (RO·) of hydroxy (HO·) radical-like intermediates. Results will be presented in different subsections, starting with the different modes of adsorption of the ROOH molecules onto the Mn^{II} active sites that lead to the two parallel ROOH *decomposition* mechanisms. Hereafter, the ethyl chain CH_3CH_2 will be denoted as R.

1. Adsorption of ROOH onto the Active Site. The first step required for the *decomposition* of the hydroperoxide intermediate is the adsorption of the molecule onto a preactivated Mn^{II} acid site, which has a proton attached to a neighboring O atom pointing to the center of a 6-ring of the channel walls. Two types of interaction are available, through H-bonds with the framework proton or by complexation with tetrahedral Mn^{II} because of its coordinative unsaturation. Depending on the ROOH orientation, there are three possible modes of adsorption, as depicted in Figure 1, leading to three different ROOH···Mn^{II} intermediates. In the first two modes of adsorption (**G1** and **G2**), the ROOH molecule is adsorbed through strong H-bonds between the framework proton and the molecular O atoms, the modes differing as to which of the two O atoms in ROOH interacts directly with the proton, and hence in the orientation of the ROOH molecule along the AFI channel; note that in **G1** and **G2**, the R−O−O−H molecular axis is oriented in opposite directions along the channel axis to enable the interaction of one O with the proton and the other with Mn. For both types of adsorption, the framework proton must reorient from its stable position located within the 6-ring that compose the 12-MR channel walls, to a position where it points toward the center of the 12-MR channel in which the ROOH molecule is located, so as to allow the H-bond interaction. We observed that no activation energy is required for this H reorientation; it takes place spontaneously, driven by the formation of H-bonds. The most stable adsorption mode corresponds to **G1** (Figure 1-left), where the H-bond is developed with the terminal oxygen atom in ROOH, resulting in an adsorption energy of −44 kJ/mol. In contrast, the development of an H-bond with the nonterminal oxygen atom in ROOH leads to a lower adsorption energy, −19 kJ/mol. These two intermediates (**G1** and **G2**) drive the ROOH *decomposition* to proceed via different reaction pathways: the orientation of the H-bonds determines the stereochemistry for the following H-transfer reaction that triggers the ROOH *decomposition*, as we shall see below: intermediate **G1** evolves into RO· intermediates (pathway A), while **G2** transforms into HO· intermediates (pathway B). Because of the different orientation of the R−O−O−H molecular axis in the two modes of adsorption, interconversion of intermediate G1 into G2 (and viceversa) requires desorption of the hydroperoxide molecule, its reorientation inside the AFI channel, and subsequent readsorption. The reorientation step may prove rate-limiting for large alkane molecules.

In intermediate **G3** (Figure 1-right), the ROOH molecule is instead directly bonded to Mn, yielding an ROOH···Mn^{II} complex. Formation of this complex has an enthalpy of −22 kJ/mol. In intermediate **G3**, the framework proton does not interact with ROOH, but is oriented in the same way as in the free

dx.doi.org/10.1021/cs2001169 |*ACS Catal.* 2011, 1, 945–955

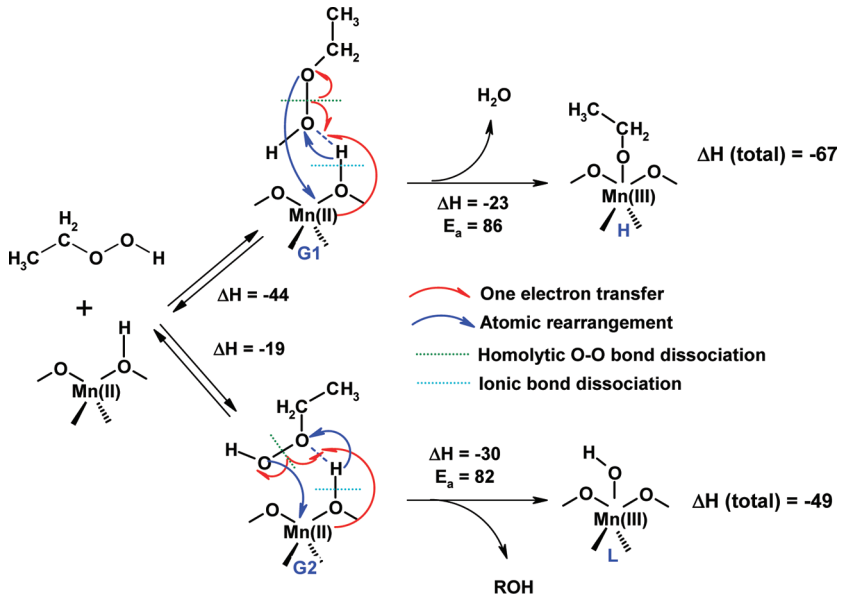

Figure 2. ROOH *decomposition* mechanism via the two alternative pathways, A (top, with formation of H_2O and RO···Mn^{III} complexes) and B (bottom, with formation of ROH and HO···Mn^{III} complexes). Dashed dark-blue lines (linking O and H atoms) indicate the H-bonds in the intermediates, along which the homolytic H-transfer in the *decomposition* mechanism occurs.

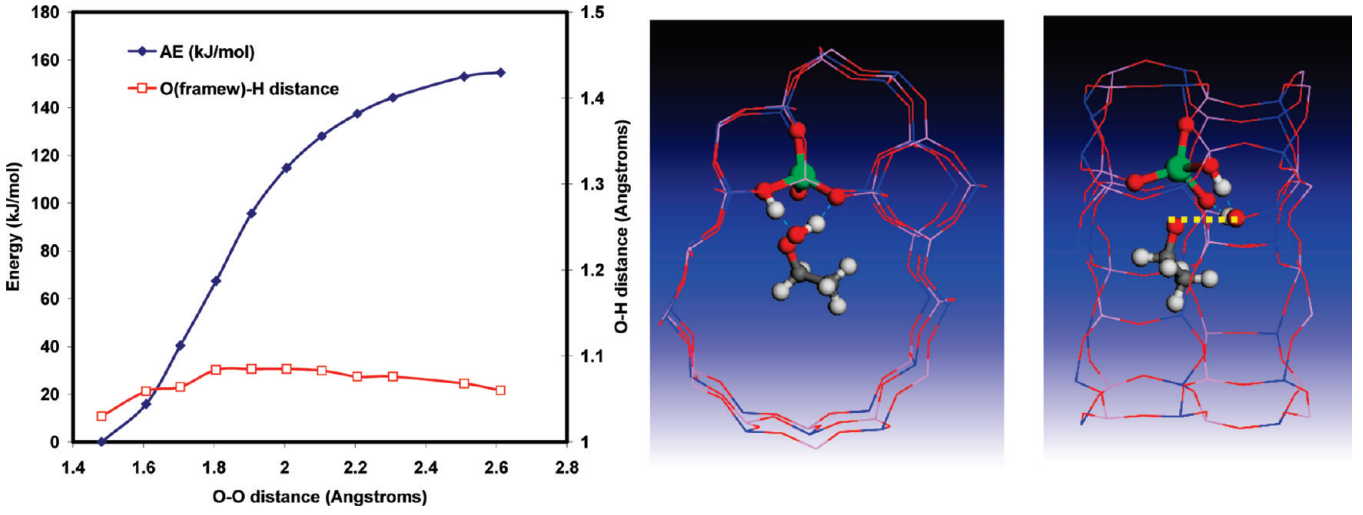

Figure 3. Left: energy profile as a function of the O−O bond distance (blue line) and evolution of the H(framework)-O(framework) distance (red line) for pathway A. Right: two views of the final product after O−O bond dissociation (at r_{OO} = 2.6 Å). A dashed yellow line indicates the O−O bond that has been dissociated.

Mn^{II} catalyst, pointing to the center of a 6-ring. However, as there is no direct interaction of the proton with the hydroperoxide molecule, **G3** cannot generate the H-transfer reaction from the framework to ROOH necessary to activate the ROOH *decomposition*, making intermediate **G3** unreactive. For the ROOH molecule to decompose, complex **G3** must rearrange to one such as **G1** or **G2** able to induce the *decomposition* mechanism for the oxidation reaction to proceed.

The adsorption energies of intermediates **G1** and **G2** have been recalculated using the B3LYP+D functional, yielding values of −49 and −23 kJ/mol, compared with −44 and −19 at B3LYP level; while, as expected, inclusion of dispersion in parametric form increases the calculated adsorption energies, its effect does not differentiate the two intermediates.

2. Pathway A: Decomposition of Intermediate G1: Mn^{II} + ROOH → Mn^{III} + RO· + H_2O. The molecular structure of intermediates **G1** or **G2**, with H-bond interaction between the framework proton and one of the oxygen atoms in ROOH, is ideal to induce a homolytic H-transfer between the atoms forming the H-bond, which initiates the ROOH *decomposition*. The mechanism for this reaction step involves several atomic and electronic rearrangements, including H-transfer, Mn oxidation, homolytic O−O bond dissociation, and complexation of the nascent radical; all these contributions are schematically depicted in Figure 2 for the two parallel pathways. The processes taking place along pathways A and B are similar; hence, we focus in greater detail on one, and in particular A, given the higher stability of intermediate **G1** from which it starts, compared to

dx.doi.org/10.1021/cs2001169 |*ACS Catal.* 2011, 1, 945–955

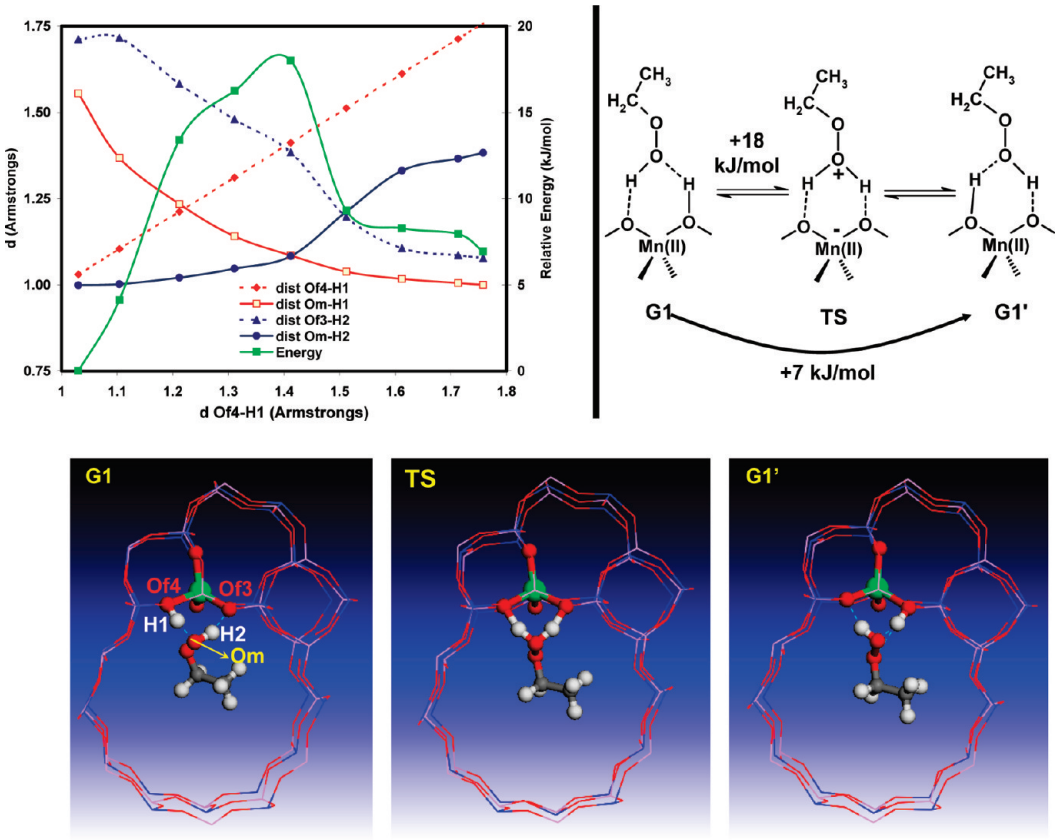

Figure 4. Variation of energy and internal coordinates as a function of the distance between framework O (Of4) and H atom (H1), with this being transferred to the ROOH molecule, for pathway A. Top-left: energy profile (green line) and evolution of representative O−H distances (red and blue lines) during the H-transfer from the framework O (Of4) to the terminal O atom in ROOH (Om). Top-right: scheme of the H-transfer reaction that takes place. Bottom: geometry of the reactant (**G1**, left), transition state (TS, middle), and product (**G1′**, right). The labeling for the different atoms whose distances are plotted in the graphic are shown in **G1**.

G2 of path B. To characterize the mechanistic details of this reaction step, we first studied the energy profile corresponding to changes of each individual atomic rearrangements: O−O bond dissociation, H-transfer from the framework to one of the molecular oxygen atoms in ROOH, and movement of ROOH toward the Mn active site through the other ROOH oxygen atom to form a complex. These results are discussed in the following subsections 2a−2c.

2a. O−O Dissociation. We first study the energy profile corresponding to an elongation of the O−O bond in ROOH. To do so, we performed a series of constrained geometry optimizations starting from the **G1** intermediate, and increasing the O−O distance (r_{OO}) in discrete steps of 0.1 Å, keeping this coordinate frozen. The energy profile as a function of r_{OO}, as well as the distance between the framework proton and framework O, are given in Figure 3-left. We observe that the energy (blue line) increases all along the reaction coordinate, up to 160 kJ/mol, in the range of r_{OO} examined, without showing a local maximum (transition state, TS). Our calculations show that the O−O bond dissociation occurs homolytically, leading to the formation of two radical species, RO· and OH·. The H(framework)-O-(framework) distance (red line) does not vary notably, indicating that the O−O bond cleavage by itself is not sufficient to induce a H-transfer from the framework to the terminal O atom in ROOH (to form H_2O with the resulting ·OH radical); a similar behavior is observed for the Mn−O distance, which is not modified upon the O−O dissociation to stabilize the RO· radical. The geometry of the final product formed is shown in Figure 3 (right), where the formation of the two radical species can be clearly observed. These results show that the O−O bond dissociation does not itself induce a rearrangement of other atoms that favor the homolytic H-transfer from the framework, suggesting that the ROOH *decomposition* is not driven only by the homolytic O−O bond cleavage.

2b. H-Transfer from Framework to ROOH. The energy profile for the H-transfer from the framework O to the hydroxylic O atom in ROOH has been calculated by stretching the framework OH bond distance at 0.1 Å intervals. The framework O is indicated as Of4, and the framework H as H1. The energy profile, as well as different representative distances, are shown in Figure 4 (top-left). We observe that an increase of the O(Of4)-H(H1) distance (dashed red line) induces a movement of the H atom toward the terminal O atom in ROOH (Om-H1 distance, solid red line), but the process takes place with an heterolytic Of4-H1 bond cleavage, without redox processes. We observe a TS, with an activation energy of 18 kJ/mol, in which the distances between the framework O atoms (Of4 and its equivalent on the other side of the Mn tetrahedron, Of3) and the two H atoms (H1 and H2) that are bonded in this TS to the terminal O atom in ROOH (dashed lines) are equal, as well as the distance between the molecular terminal O atom (Om) and the two H atoms (solid lines). In this TS (Figure 4, bottom-middle), the spin of Mn is still 4.82, corresponding to Mn^{II},

dx.doi.org/10.1021/cs2001169 |*ACS Catal.* 2011, 1, 945–955

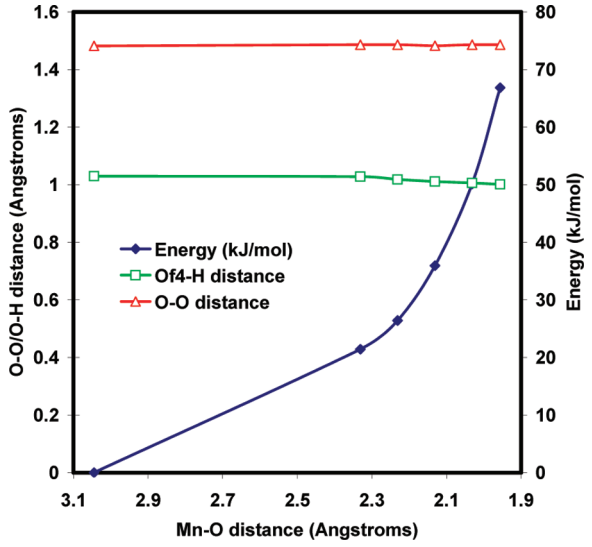

Figure 5. Variation of energy and bond distances as a function of the Mn−O distance (pathway A); ROOH approaches Mn^{II} through the nonterminal O atom. The energy profile is displayed as the blue line, while the evolution of the H(framework)-O(framework) (Of4-H) and intramolecular O−O distances (O−O) are shown as green and red lines, respectively.

showing the formation of an ionic pair $RO{-}OH_2^+\cdots(Mn^{II})^-$ (Figure 4, top-right, TS). Passing this activation barrier causes a reduction of the Of3-H2 distance and a consequent increase of the Om-H2 distance, showing the transfer of H2 back to the framework, yielding again the ROOH molecule, and Mn^{II} sites, but with the proton being attached to a different framework O attached to a 6-ring (Of3) (**G1′**) (Figure 4, bottom-right). This process is schematically shown in Figure 4, top-right. Such a H^+ hopping process requires a low activation energy (18 kJ/mol), and has a reaction enthalpy of +7 kJ/mol, which is slightly endothermic because of the lower stability of the proton attached to the new framework O position (Of3), compared to Of4 (**G1**).

The O−O bond distance remains almost constant along all the process, showing that such a heterolytic H-transfer is not able to induce the O−O bond dissociation, as expected because of the high energy cost of the latter; the same occurs for the Mn−O distance. The energies involved in the H-transfer are much lower than those required for the O−O bond dissociation, suggesting that such proton jumps may occur with relatively high frequency during the reaction cycle, but are ineffective in terms of the catalytic oxidation cycle.

2c. Approach of ROOH to Mn. The third reaction coordinate corresponds to the approach of the ROOH molecule to the Mn active site to form a complex through the RO group. We selected as the reaction coordinate the distance between Mn and the nonterminal O atom in ROOH (underlined), which is the one that will bind Mn upon the ROOH *decomposition* via pathway A, freezing this distance at intervals of 0.1 Å and relaxing the rest of the internal coordinates. The goal of this study is to determine if the formation of this complex could induce the O−O bond dissociation by direct electron transfer from Mn^{II} to ROOH, to yield RO· and OH^- and stabilizing the resulting RO· radical. The energy profile for this reaction coordinate is given in Figure 5. The energy increases up to 67 kJ/mol, without showing any evidence of a change in curvature that could suggest a TS. The approach of ROOH to the Mn active site does not induce either a O−O bond dissociation or an H-transfer, as shown by the nearly constant value of these distances (Figure 5, green and red lines) throughout the reaction profile.

2d. O−O Bond Dissociation in $RO{-}OH_2^+\cdots(Mn^{II})^-$. We have observed in section 2b that heterolytic H-transfer has a low activation barrier of 18 kJ/mol, and is expected to occur with relatively high frequency. It is therefore of interest to examine whether the O−O bond cleavage can occur more readily in the protonated intermediate $ROOH_2^+$ than in the neutral hydroperoxide ROOH. To this end, we repeated the calculations discussed in section 2a for the O−O bond cleavage, but starting from a configuration where the proton had been transferred to the terminal O in ROOH. The energy profile for this O−O bond dissociation is essentially the same as the initial one, where the H atom was bonded to the framework, showing that an heterolytic H-transfer does not facilitate the O−O bond dissociation in the ROOH *decomposition* reaction.

In summary, the initial set of calculations discussed in sections 2a−2d demonstrates that the modification of a single internal coordinate is not able to induce the complex rearrangement required for the ROOH decomposition to occur, showing that the ROOH *decomposition* must involve a concerted mechanism in which all the atomic and electronic rearrangements take place simultaneously. In addition, these initial results show that the most energy-demanding process in this reaction step corresponds to the O−O bond cleavage.

2e. Estimation of the TS of the Concerted Mechanism. To determine the transition state and activation energy for the ROOH *decomposition*, we have to study the energy profile for a mechanistic pathway in which the three bond distances discussed above (O−O, O···H, and O···Mn) vary simultaneously. To do so, we have initially identified the partial TSs for each of these internal coordinates. The goal of this part of our work is to identify an approximate TS to be subsequently refined by TS search techniques based on the Hessian matrix, which needs to start in a region of coordinate space close enough to the TS for the Hessian to have the correct curvature.

We started from the most energetically demanding atomic rearrangement that, as discussed earlier, corresponds to the O−O bond dissociation. We have already observed in section 2a that the O−O bond dissociation does not by itself induce the overall ROOH *decomposition*, that is, the H-transfer and the radical complexation by Mn. To determine the partial transition state for this particular reaction coordinate, we followed a similar strategy as before, keeping the O−O bond distance frozen at intervals of 0.1 Å; however, in this case, two different initial configurations were studied, (i) that corresponding to the reactants, where the O−O distance was increased by 0.1 Å steps so as to move toward the TS, and (ii) that corresponding to the products (RO· + H_2O), in this case decreasing the O−O distance. In the reactant configuration, the O−O bond is present, and the proton is attached to the framework, and so Mn is in the reduced (II) oxidation state and does not form a complex with ROOH, while in the product configuration, the O−O bond has been dissociated, and the H atom has been transferred to the terminal molecular OH group, so Mn is in the oxidized state and forms the complex with RO·. The partial TS for the O−O reaction coordinate, TS_{OO}, has been chosen as the O−O distance at which the energy profile of the two configurations (reactants and products) intersects, which corresponds to r_{OO} = 1.76 Å (Figure 6-left). At O−O distances smaller than this value, the configuration obtained starting from the reactants, with Mn

dx.doi.org/10.1021/cs2001169 |*ACS Catal.* 2011, 1, 945–955

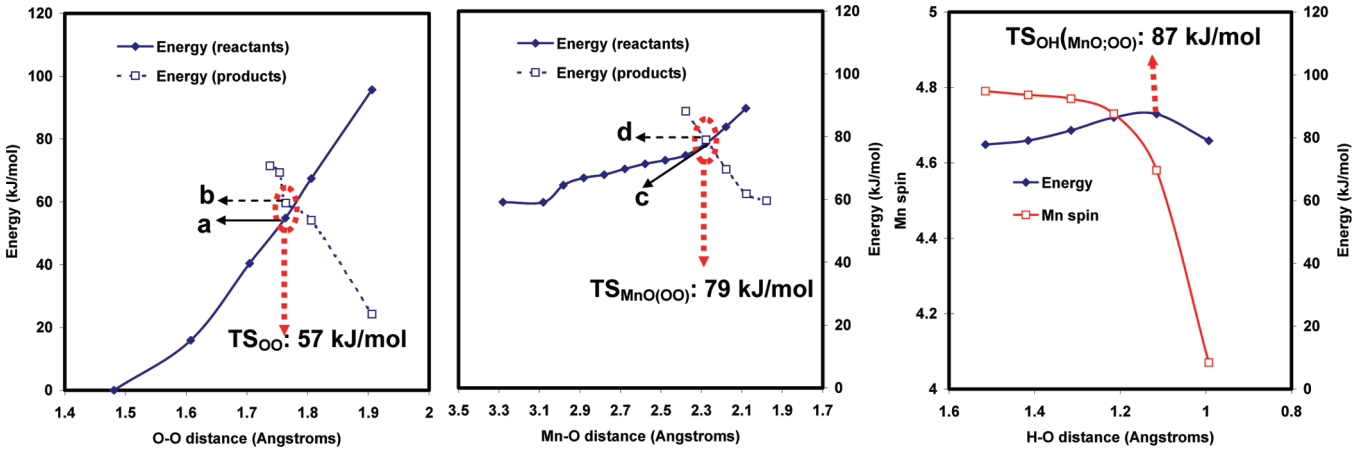

Figure 6. Partial contribution to TS and activation energy for the ROOH *decomposition* via pathway A from individual internal coordinates: O−O (left), Mn−O (middle), and H−O (right). The energy obtained starting from both reagent-like (solid blue lines) and product-like (dashed blue lines) conformations are reported; the red line in the O−H diagram is the Mn spin.

in oxidation state of +2, is stable, while at longer O−O distances the system is stable in a product-like configuration, resulting in the oxidation of the active site to Mn^{III}.

We assumed at this point that the lowest energy pathway for the ROOH *decomposition* involving the other necessary atomic rearrangements, H-transfer and Mn complexation, takes place at this particular O−O bond distance of 1.76 Å. This partial TS involves a contribution to the activation energy from the O−O bond cleavage of 57 kJ/mol, which does not take into account the energy cost of the other atomic rearrangements.

Having determined the partial TS for the O−O bond dissociation, we varied the next internal coordinate, chosen as the distance between the ROOH molecule and the active site to form a complex with Mn, since we observed in the previous sections that this atomic rearrangement involves a higher energy than the H-transfer reaction. We followed the same strategy as before, studying the energy profile as a function of the Mn-O(ROOH) separation by modifying the distance between the nonterminal O atom in ROOH (underlined) and the Mn active site, with the system in the two configurations (reactants and products) and the O−O bond distance frozen at TS_{OO} (r_{OO} = 1.76 Å). In the configuration corresponding to the reactants, the Mn−O distance was gradually decreased in 0.1 Å intervals so as to form the complex, while in the configuration of the products, the Mn−O distance was increased, thus both moving toward the TS. In both cases, not only the Mn−O bond distance was kept frozen, to provide the energy profile for the Mn−O bond formation, but also the O−O bond distance at 1.76 Å (TS_{OO}). The results show that the two energy profiles, corresponding to the reactant and product configurations, intersect at an Mn−O distance of 2.28 Å (TS_{MnO}). We identify this as the partial TS configuration for the Mn−O bond formation at the partial TS for the O−O bond dissociation. The activation energy for these two atomic rearrangements is now 79 kJ/mol, corresponding to an increase of 22 kJ/mol upon the Mn−O bond formation with respect to the O−O bond dissociation activation energy.

Finally, having identified these two partial TS coordinates, we studied the last atomic rearrangement, namely, the H-transfer from the framework to the terminal O atom to form H_2O which, as we observed above, corresponds to the least energy-demanding contribution. We set as reaction coordinate the distance between the terminal O atom in ROOH (underlined) and the H atom. In this case, since this is the last atomic rearrangement required for completion of the overall ROOH *decomposition*, the PES starting from reactants and products is the same. A decrease of the H−O distance leads to the transformation of the reactants into the products. The final energy profile for this H-transfer is shown in Figure 6 (right), where we observe that the overall TS corresponds to an H−O distance of 1.12 Å, with a corresponding activation energy of 87 kJ/mol; this estimated energy corresponds to the overall activation energy for the whole process of the ROOH *decomposition* step via pathway A. In agreement with previous findings, we observe that this H-transfer involves the lowest contribution to the activation energy, 8 kJ/mol. The variation of the spin of Mn along the H-transfer coordinate (red line) shows the oxidation of Mn^{II} to Mn^{III}, the final Mn oxidation state after the ROOH *decomposition*.

The results discussed in this section show that the hydroperoxide decomposition and simultaneous oxidation of Mn to (III) oxidation state occur upon homolytic transfer of H from the framework to the molecule, but this process requires a molecular structure in which the intramolecular O−O bond is stretched; otherwise, it occurs as an heterolytic process, as seen in section 2c.

2f. Refinement of the TS Structure. The previous set of calculations allowed us to obtain an estimate of the TS structure and activation energy for the hydroperoxide *decomposition*. Because of the complexity of the TS, where three different atomic rerrangements, H-transfer, O−O bond dissociation, and complex formation, are involved, the final structure of the TS was refined by second-derivative methods after calculating the Hessian, ensuring that only one negative frequency was observed in the TS. Indeed, numerical calculation of the Hessian at the TS geometry identified in section 2e shows that one imaginary mode is present (υ = −730 cm^{-1}) connecting reagents and products. There is a second imaginary mode (υ = −44 cm^{-1}), with clearly distinguishable value that makes it of secondary importance but which requires refinement via eigenvalue following methods.

The structure of the final TS is displayed in Figure 7 (top), which gave an associated activation energy of 86 kJ/mol. This TS is very similar to the one estimated following the strategy outlined in section 2e, both in the structure (to within the step size) and in the activation energy (a difference of 1 kJ/mol). The final TS has O−O, Mn−O, and H−O distances of 1.74, 2.26,

dx.doi.org/10.1021/cs2001169 |*ACS Catal.* 2011, 1, 945–955

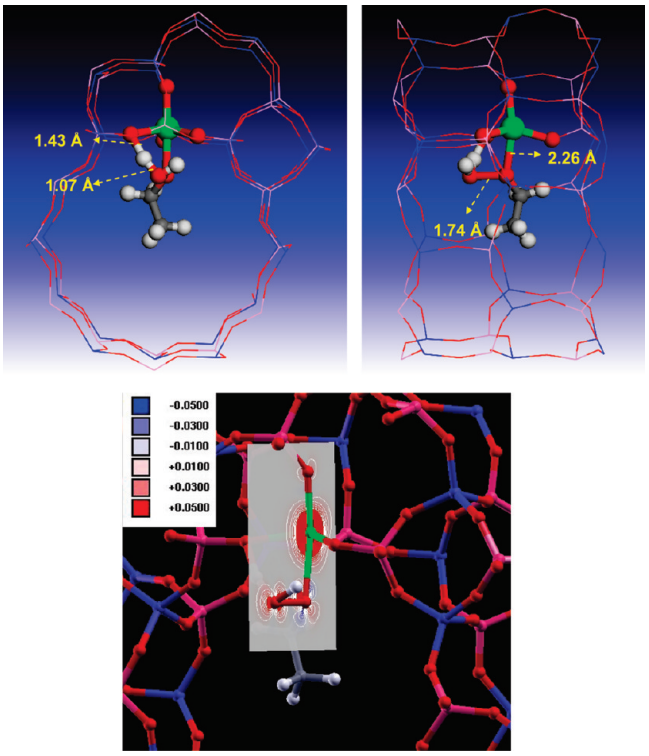

Figure 7. Structure (top) and spin density map (bottom) of the transition state (after refinement) for the ROOH *decomposition* to form H_2O and RO· radical-like species via pathway A.

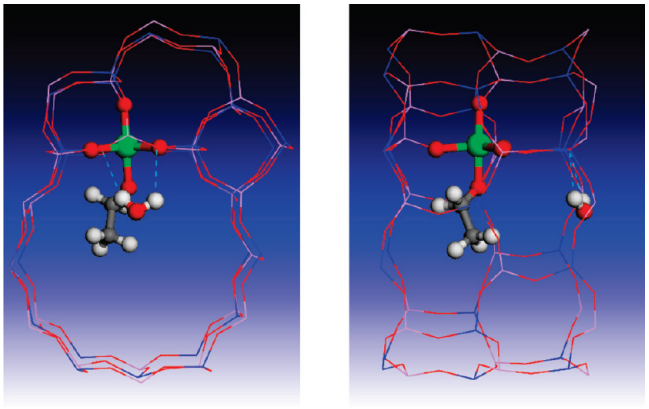

Figure 8. Structure of the products of the ROOH *decomposition* via pathway A: $Mn^{III}\cdots OR$ complex and H_2O.

and 1.07 Å, respectively (compared to 1.76, 2.28, and 1.12 Å from the estimated TS); we note that the proton is shared between the framework and the terminal OH group of ROOH. The spin density map of this TS (Figure 7-bottom) shows that the spin is concentrated on the Mn active site and on the O atoms in ROOH, demonstrating the homolytic cleavage of the O—O bond. In this reaction step, one electron is transferred from Mn to the nonterminal O atom in ROOH to yield an RO· radical-like species stabilized by binding to Mn; the hydroxylic O atom forms a covalent H—O bond with the transferred H, yielding a molecule of H_2O.

The overall reaction enthalpy for this ROOH *decomposition* mechanism was calculated as −23 kJ/mol, by full geometry optimization of the reactants and products. The products resulting from this ROOH *decomposition* are H_2O and an $Mn^{III}\cdots OR$ complex, whose structures are shown in Figure 8. The H_2O molecule forms H-bonds with framework O atoms. The formation energy of the $Mn^{III}\cdots OR$ complex was calculated as −67 kJ/mol, by subtracting the energy of the system with the free RO· radical (located in the middle of the channel) to the energy of the complex. This high value shows the strong stabilization of the RO· radical achieved by binding to the Mn^{III} active site.

3. Pathway B: Decomposition of Intermediate G2: Mn^{II} + ROOH → Mn^{III} + HO· + ROH. Having studied in detail the *decomposition* mechanism of ROOH from intermediate **G1** to form H_2O and an RO· radical-like species (pathway A), we employed the same methodology to study the alternative ROOH *decomposition* mechanism, starting from intermediate **G2**, where the H-bond is developed between the framework proton and the nonterminal O atom in ROOH (underlined), to form ROH and an $Mn^{III}\cdots OH$ complex (pathway B). We performed the same set of calculations as before, first scanning the energy profile for a change in each of the 3 relevant internal coordinates (O—O, O···H, and O···Mn). The results are similar to those of pathway A, with the only quantitative difference relating to the heterolytic H-transfer reaction, which in pathway B requires a higher activation energy of 29 kJ/mol (compared to 18 kJ/mol in pathway A). None of the internal coordinates by itself can induce the overall reaction, hence pathway B also requires a concerted mechanism.

The estimate of the TS has been obtained by identifying the value of each internal coordinate in turn, in which the PES of reagents and products intersect, starting from the O—O distance. The calculated energies are shown in Figure 9. The partial TS corresponds to an O—O distance of 1.76 Å, with an activation energy of 59 kJ/mol, both very similar to the values found for pathway A (1.76 Å and 57 kJ/mol). The Mn—O contribution corresponds to a distance between Mn and the terminal molecular O atom (ROOH) of 2.25 Å, with an activation energy of 66 kJ/mol. The final H-transfer to the nonterminal O (ROOH), with the other two reaction coordinates frozen at their partial TS values, has a final activation barrier of 80 kJ/mol (corresponding to an increase of 14 kJ/mol), which corresponds to the overall activation energy estimated for this ROOH *decomposition* pathway; the distance between the H atom and the nonterminal O is 1.21 Å. The evolution of the spin of Mn in this final step (Figure 9-right) shows again the oxidation of Mn upon this ROOH *decomposition* pathway.

The structure of the TS was refined by second-derivative methods, ensuring the presence of only one imaginary mode. The structure of the final TS is shown in Figure 10, where we can clearly observe that the proton is shared between the framework and the nonterminal ROOH O atom. The activation energy associated with this TS, 82 kJ/mol, is very similar to that estimated above (80 kJ/mol), as is the structure. The spin density map (Figure 10-bottom) indicates that the spin density is mainly localized on the Mn active site and on the O atoms in ROOH, showing the homolytic nature of the O—O bond cleavage: one electron is transferred to the terminal O atom to form an OH· radical that will bind Mn, while the other (together with the electron donated by Mn) forms a new O—H bond with the H atom from the framework to yield ROH.

The total reaction enthalpy for this ROOH *decomposition* mechanism was calculated as −30 kJ/mol; the mechanism yields ROH and an $Mn^{III}\cdots OH$ complex. The formation energy of the $Mn^{III}\cdots OH$ complex was calculated as −66 kJ/mol, very similar

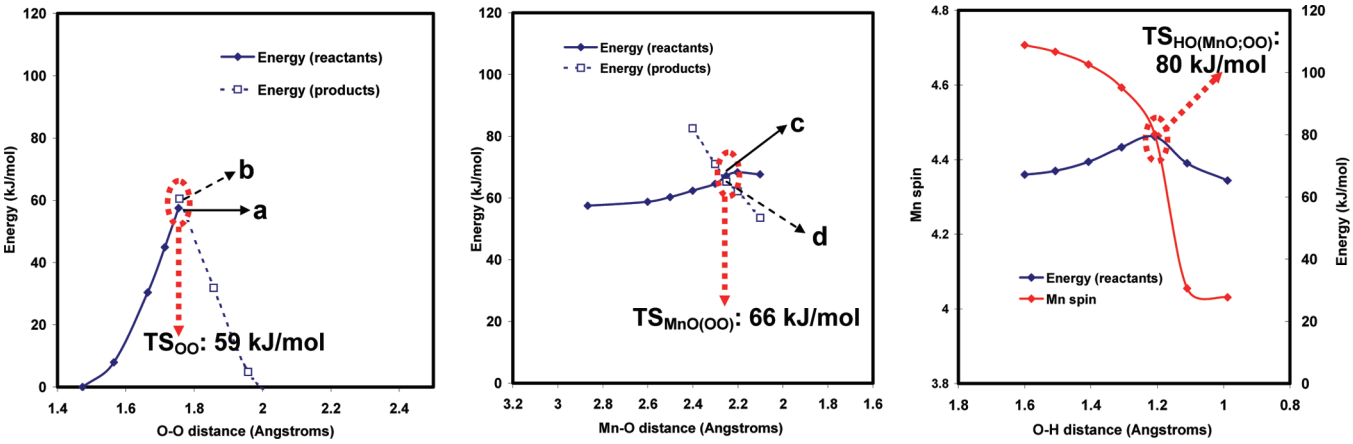

Figure 9. Partial contribution to TS and activation energy for the ROOH *decomposition* via pathway B from individual internal coordinates: O−O (left), Mn−O (middle), and H−O (right). The energy obtained starting from both reagent-like (solid blue lines) and product-like (dashed blue lines) conformations are reported; the red line in the O−H diagram is the Mn spin.

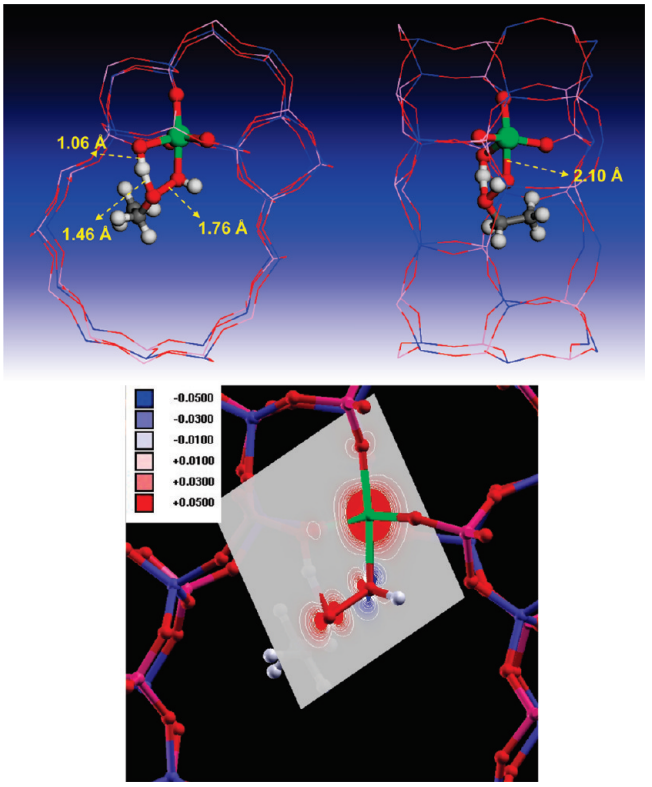

Figure 10. Structure (top) and spin density map (bottom) of the transition state (after refinement) for the ROOH *decomposition* to form ROH and HO· radical-like species via pathway B.

to that of complex $Mn^{III}\cdots OR$, again showing the crucial contribution of the interaction between oxo-type radicals and Mn^{III} in the energetic balance of this reaction step.

Similarly to the adsorption energies of the starting intermediates, we have recalculated the reaction enthalpies of pathways A and B using the dispersion corrected B3LYP+D functional. The reaction enthalpies change from −23 to −28 kJ/mol (pathway A) and from −30 to −35 kJ/mol (pathway B). Once more, the effect of dispersion is not pronounced: the atomic composition of reactants and products is identical, and dispersion forces yield similar contributions to both, that largely cancel out in reaction energies. For this reason, the effect of dispersion has not been calculated for all other intermediate species identified in the reaction cycle.

DISCUSSION

First, let us consider some methodological issues. The reaction pathway leading to decomposition of the hydroperoxide intermediate occurs with simultaneous changes of three internal coordinates: the Mn−O, O−O, and O−H distances of the bonds that are formed or cleaved in this elementary reaction step. Partial interpolations in which only one of these three bond distances is varied do not lead to the desired product, showing the concerted nature of the mechanism. Under these circumstances, obtaining even a rough guess of the TS structure, to be refined with second derivative techniques, has revealed itself to be a demanding task. In our study, we factorized the problem, and identified partial TS coordinates in the energy surface of each internal coordinate, in order of decreasing bond energy involved (calculated in an earlier stage of the study). We started therefore from the O−O bond cleavage, followed by Mn−O and finally O−H distances. This procedure allowed us to obtain a working approximation for the TS in the *decomposition* of the hydroperoxide intermediate. Indeed, the subsequent refinement by second-derivative methods yielded very similar structures and activation energies. Such second-derivative-based techniques to determine TSs are still uncommon under periodic boundary conditions because of the high cost of computing the Hessian matrix of these systems. However, in our case, Hessian-based techniques are required because of the mechanistic complexity of the reaction studied, which is not suitable for simpler methods based on for instance Nudged Elastic Bands (NEB); similarly, adiabatic molecular dynamics simulations, even using a very high temperature, are impractical because of the high activation barriers. Unbiased and more efficient simulation methods to locate TSs are being developed, such as Metadynamics-based techniques; however, these still rely on the a priori definition of a set of variables that span the reactive subspace, and their cost increases exponentially with the number of reactive variables, so that their application with quantum chemical Hamiltonians is still limited in practice to one or two active variables. Therefore, the simplified strategy we have followed may become useful for

dx.doi.org/10.1021/cs2001169 |*ACS Catal.* 2011, 1, 945–955

searching complex transition states where several internal coordinates vary simultaneously in a concerted mechanism, as in our case.

The ROOH *decomposition* involves a complex mechanism which includes electron transfer, O−O bond dissociation, H-transfer, and Mn complexation. Our results have shown that these atomic rearrangements take place through a concerted mechanism—no single rearrangement is able to induce the completion of the reaction step. The activation energies required for this process were found to be 86 and 82 kJ/mol for pathways A and B, respectively. These values are reasonably close to the experimental activation energy found for the same reaction step in the aerobic oxidation of cyclohexane catalyzed by MnAPO-5, which was found to be 105 ± 10 kJ/mol.[14] Although we have not studied the same hydrocarbon (ethane in our case), we consider that the electronic mechanism whereby the reaction takes place should be essentially the same, regardless of the hydrocarbon size, thus giving confidence in the reliability of the computational methodology we have employed; however, we should note that slight differences in the activation energies are expected because of the presence of secondary (rather than primary) C atoms in cyclohexane, as well as to its larger size that may prevent an effective complexation of the resulting RO· radical product to Mn^{III}, thus increasing the activation energy. The high activation energy found for this step of 86 kJ/mol, which is the highest in all the propagation cycle,[24] suggests this to be the rate-limiting step in the overall reaction, as was observed experimentally.[14]

We have found that two different reaction pathways can take place for the ROOH *decomposition*, one of which (pathway B) has not been proposed before for this type of system. Which of the two mechanisms occurs depends on the stereochemistry of the initial adsorption of the ROOH molecule onto the active site, that is, which of the two oxygen atoms in ROOH forms an H-bond to the framework proton, since this H-bonding geometry determines the stereochemistry of the consequent H-transfer reaction. The adsorbed intermediate in which the framework proton is H-bonded to the hydroxylic O (**G1**) is much more stable (by 25 kJ/mol), suggesting that this will be the main intermediate formed, and thus suggesting a preferential occurrence of pathway A compared to pathway B in the oxidation reaction.

The total reaction enthalpy for the ROOH *decomposition* mechanism, including adsorption of ROOH and subsequent *decomposition*, is more exothermic if the reaction takes place via pathway A (−67 kJ/mol) than via pathway B (−49 kJ/mol) (Figure 2). These energy differences can be explained by the energetic difference between CH_3CH_2O· and ·OH radicals as well as between CH_3CH_2OH and H_2O molecules. The O−H bond energy, as calculated at the same level of theory (DFT-B3LYP; XO-H → XO· + H·), was found to be +442 and +500 kJ/mol for CH_3CH_2OH and H_2O, respectively, showing a higher stability of CH_3CH_2O· than HO· radicals. These energy values also indicate a higher bond energy of the O−H bonds in H_2O than in CH_3CH_2OH, thus explaining the more exothermic reaction enthalpy via pathway A, where more stable species (H_2O and CH_3CH_2O·) are formed.

The Mn active sites have been found to play an essential role in this step. Their ability to undergo redox processes, and so to be oxidized upon the ROOH *decomposition*, enables the homolytic transfer of an H atom from the framework, necessary to form a covalent bond with the radical O atom resulting from the homolytic dissociation of the O−O bond in ROOH. Nevertheless, this is not the only role for Mn in this reaction. We have observed that the ROOH *decomposition* cannot take place if the radicals formed (RO· or ·OH) end up free inside the channel; section 2d showed that the *decomposition* cannot evolve if only the O−O bond is dissociated and the H atom is transferred. The stabilization (by 66 kJ/mol) of the nascent radicals by complexation to Mn is crucial for this mechanism. This action of Mn is enabled by its coordinative unsaturation when embedded in aluminophosphate networks, where it occupies tetrahedral positions, and as such can readily increase its coordination number, as well as by the high Lewis acidity of Mn^{III} (d^4) ions, which have a stronger electron affinity than Mn^{II} (d^5).

Noncatalytic ROOH *decomposition* pathways can be ruled out because of their very high activation barriers. Gas-phase *decomposition* of ROOH into RO· + ·OH has a reaction enthalpy of 187 kJ/mol, while *decomposition* into ROO· and H· requires an even higher energy of 362 kJ/mol (these values were determined in vacuo, using the same level of theory (DFT-B3LYP)). These high energies will prohibit an appreciable occurrence of noncatalytic ROOH *decomposition* pathways compared to those assisted by Mn, which require a much lower activation energy (less than 90 kJ/mol), confirming the essential role of the Mn active sites in this reaction step.

The complexes with the oxo radical-like species formed as a consequence of the ROOH *decomposition*, $Mn^{III}\cdots OR$ and $Mn^{III}\cdots OH$, will be responsible for the activation of new hydrocarbon molecules by means of H-transfer reactions to the radical O atom, leading to the *propagation* reactions that will be reported in detail in a subsequent paper.[29]

CONCLUSIONS

In the present work, we have applied computational methods to find the transition state and activation energies for the *decomposition* of the hydroperoxide intermediate ROOH during the aerobic oxidation of hydrocarbons catalyzed by MnAPO-5. Our computational protocol is based on a search by constrained geometry optimizations of the partial transition states corresponding to each of the internal coordinates modified during the ROOH *decomposition*. Final refinement of the TS by second-derivative methods showed very similar structures and activation energies, demonstrating the good performance of our computational strategy. The calculated activation energies are in good agreement with the experimental data available.

Two alternative pathways for the ROOH *decomposition* have been identified: one that leads to the formation of water (HOH) and $Mn^{III}\cdots OR$ complexes (pathway A) and another that yields the alcohol (ROH) and $Mn^{III}\cdots OH$ complexes (pathway B). The occurrence of one or the other mechanism depends on the initial mode of adsorption of the ROOH hydroperoxide onto the active site. The development of H-bonds between the framework H atom and the terminal (pathway A) or nonterminal (pathway B) O atom in ROOH determines the stereochemistry of the subsequent H-transfer, and hence the pathway whereby the ROOH *decomposition* takes place. A more stable adsorption energy has been found for the former mode of adsorption, suggesting that pathway A predominates. Noncatalytic pathways have been shown to require much higher activation energies, ruling out their significant occurrence compared to Mn-assisted routes.

The *decomposition* mechanism takes place through a concerted mechanism, in which the electron transfer, the H-transfer, the O−O bond dissociation, and the approach of the resulting oxo-radical to Mn so as to form a complex must take place at the same time. Atomic rearrangements of any of these components alone cannot induce the completion of the *decomposition* mechanism. The Mn active sites play an essential role, not only in enabling the homolytic H transfer so as to form a new O−H covalent bond with the ROOH oxygen atom, but also in stabilizing the nascent radicals by complexation due to the coordinative unsaturation of tetrahedral Mn^{III} sites embedded in aluminophosphate frameworks.

AUTHOR INFORMATION

Corresponding Author

*E-mail: lhortiguela@icp.csic.es (L.G.-H.), f.cora@ucl.ac.uk (F.C.).

Funding Sources

L.G.H. acknowledges funding from EPSRC (Grant EP/D504872).

ACKNOWLEDGMENT

We are grateful to Sir John Meurig Thomas, Gopinathan Sankar, and Claudio M. Zicovich-Wilson for helpful discussions. The authors acknowledge the use of the UCL Legion High Performance Computing Facility, and associated support services, in the completion of this work.

REFERENCES

(1) Wilson, S. T.; Lok, B. M.; Flanigen, E. M. U.S. Patent 4310440, 1982.
(2) Saadoune, I.; Corà, F.; Alfredsson, M.; Catlow, C. R. A. *J. Phys. Chem. B* **2003**, *107*, 3012–3018.
(3) Corà, F.; Sankar, G.; Catlow, C. R. A.; Thomas, J. M. *Chem. Commun.* **2002**, 734–735.
(4) Thomas, J. M. *Angew. Chem., Int. Ed.* **1999**, *38*, 3589–3628.
(5) Arends, I. W. C. E.; Sheldon, R. A.; Wallau, M.; Schuchardt, U. *Angew. Chem., Int. Ed. Engl.* **1997**, *36*, 1144–1163.
(6) Hartmann, M.; Ernst, S. *Angew. Chem., Int. Ed.* **2000**, *39*, 888–890.
(7) Thomas, J. M.; Raja, R.; Sankar, G.; Bell, R. *Nature* **1999**, *298*, 227–230.
(8) Modén, B.; Oliviero, L.; Dakka, J.; Santiesteban, J. G.; Iglesia, E. *J. Phys. Chem. B* **2004**, *108*, 5552–5563.
(9) Modén, B.; Zhan, B.-Z.; Dakka, J.; Santiesteban, J. G.; Iglesia, E. *J. Phys. Chem. C* **2007**, *107*, 1402–1411.
(10) Raja, R.; Sankar, G.; Thomas, J. M. *Angew. Chem., Int. Ed.* **2000**, *39*, 2313–2316.
(11) Vanoppen, D. L.; De Vos, D. E.; Genet, M. J.; Rouxhet, P. G.; Jacobs, P. A. *Angew. Chem., Int. Ed. Engl.* **1995**, *34*, 560–563.
(12) Luna, F. J.; Ukawa, S. E.; Wallau, M.; Schuchardt, U. *J. Mol. Catal. A: Chem.* **1997**, *117*, 405–411.
(13) Raja, R.; Sankar, G.; Thomas, J. M. *J. Am. Chem. Soc.* **1999**, *121*, 11926–11927.
(14) Modén, B.; Zhan, B.-Z.; Dakka, J.; Santiesteban, J. G.; Iglesia, E. *J. Catal.* **2006**, *239*, 390–401.
(15) Concepción, P.; Corma, A.; López-Nieto, J. M.; Pérez-Pariente, J. *App. Catal., A* **1996**, *143*, 17–28.
(16) Zhou, L.; Xu, J.; Chen, C.; Wang, F.; Li, X. *J. Porous Mater.* **2008**, *15*, 7–12.
(17) Dugal, M.; Sankar, G.; Raja, R.; Thomas, J. M. *Angew. Chem., Int. Ed.* **2000**, *39*, 2310–2313.
(18) Raja, R.; Sankar, G.; Thomas, J. M. *Chem. Commun.* **1999**, 829–830.
(19) Raja, R.; Thomas, J. M.; Sankar, G. *Chem. Commun.* **1999**, 525–526.
(20) Thomas, J. M.; Raja, R.; Sankar, G.; Bell, R. *Acc. Chem. Res.* **2001**, *34*, 191–200.
(21) Sheldon, R. A.; Kochi, J. K. *Metal-Catalysed Oxidations of Organic Compounds*; Academic Press: New York, 1981.
(22) Hill, C. L. *Activation and Functionalisation of alkanes*; John Wiley & Sons, Inc.: New York, 1989.
(23) Black, J. F. *J. Am. Chem. Soc.* **1978**, *100*, 527–535.
(24) Gómez-Hortigüela, L.; Corà, F.; Sankar, G.; Zicovich-Wilson, C. M.; Catlow, C. R. A. *Chem.—Eur. J.* **2010**, *16*, 13638–13645.
(25) Gómez-Hortigüela, L.; Corà, F.; Catlow, C. R. A. *ACS Catalysis* **2011**, *1*, 18–28.
(26) Dovesi, R.; Saunders, V. R.; Roetti, C.; Orlando, R.; Zicovich-Wilson, C. M.; Pascale, F.; Civalleri, B.; Doll, K.; Harrison, N. M.; Bush, I. J.; D'Arco, Ph.; Llunell, M. *CRYSTAL09*; University of Torino: Torino, Italy, 2009.
(27) Grimme, S. *J. Comput. Chem.* **2006**, *27*, 1787–1799.
(28) Ugliengo, P.; Zicovich-Wilson, C. M.; Tosoni, S.; Civalleri, B. *J. Mater. Chem.* **2009**, *19*, 2564–2572.
(29) Gómez-Hortigüela, L.; Corà, F.; Catlow, C. R. A., manuscript in preparation.